Heterojunction GaAs/AlGaAs Terahertz Detectors

A. G. U. Perera, M. I. Stockman, G. Hastings,
M. B. M. Rinzan, and S. G. Matsik
Dept. of Physics and Astronomy
Georgia State University
Atlanta, GA 30303

H. C. Liu, Z. R. Wasilewski,
and M. Buchanan
Institute for Microstructural Sciences
National Research Council
Ottawa K1A 0R6, Canada

***Abstract*— The THz region is of considerable interest for many applications, in particular for applications in astrophysics and biophysics. The limits on Al growth fraction have restricted previous devices to a 3.1 THz (96.8 μm, 103 cm^{-1}) threshold. A new approach, replacing doped GaAs emitters with doped $Al_xGa_{1-x}As$, overcomes this limit, extending the threshold to lower frequencies. Here, results are reported on a p-$Al_xGa_{1-x}As$/GaAs heterojunction interfacial workfunction internal photoemission (HEIWIP) detector operating in the 30-2.3 THz (10-128 μm)range. The spectra for a detector using this approach have a strong response for frequencies lower than 150 THz with a threshold of 2.3 THz. The peak frequency at 9.6 THz ($\lambda = 31$ μm) gave a response of 7.3 A/W and $D^* = 5.3 \times 10^{11}$ Jones. A BLIP temperature of 20 K was obtained. As future developments, possible response enhancing mechanisms such as surface plasmon (SP) effects, alternate material systems, and a possible dual band detector are considered.**

I. Introduction

Astrophysics has traditionally been an important area for THz applications. The large number of spectral lines associated with molecules and the ability of THz radiation to travel through dust clouds have made this range increasingly important for the study of numerous astronomical objects. Also recently, extension of FTIR difference spectroscopy techniques down to $\sim$ 6 THz (200 cm^{-1}) have been used for studies of biological systems.[1], [2], [3] In these biophysical measurements silicon bolometers were used. Silicon bolometers have a very long time constant, which makes these biophysical FTIR measurements problematic because considerable signal averaging is required in these experiments. Given the bolometer time constant, the low frequency biophysical FTIR measurements can take many hours to days to complete. This is quite impractical and the development of new and "fast" THz detector technologies should positively impact the feasibility of these biophysical FTIR measurements. In addition to these applications, the recent developments in THz sources and imaging systems have led to renewed interest in detectors. The work presented here is aimed at developing fast broadband THz detectors with multiple applications. The quantum well photodetectors (QWIPs) have recently extended the f_0 to $\sim$ 5 THz.[4] However, it is still below the response region of HEIWIPs. In QWIPs, decreasing the frequency further requires the doping density to be decreased to reduce dark current, but this lowers the absorption and therefore the sensitivity. The work presented here involves a different approach using free-carrier absorption and an interfacial workfunction to operate in the THz regime.

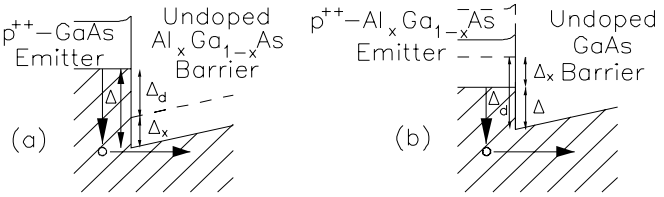

Fig. 1. A partial band diagram showing the detection mechanism in HEIWIP detectors. (a) In the standard design Doped GaAs was used as the emitter and undoped AlGaAs was used for the barrier. (b) To extend the threshold doped AlGaAs was used as the emitters while undoped GaAs forms the barriers. The dashed lines indicate the location of the fermi level and band edge if the AlGaAs layer were GaAs.

A. Basic Detector Design

The basic design of an Interfacial Workfunction Internal Photoemission (IWIP) detector consists of a sequence of alternating heavily doped emitter layers and undoped barrier layers.[5] Depending on whether the layers have the same or different compositions, the detectors are classified as Homojunction (HIWIP)[6] or HEterojunction (HEIWIP) Interfacial Workfunction Internal Photoemission detectors[7]. The detection mechanism is the same in both the HIWIP and HEIWIP detectors. The radiation is absorbed in the highly doped emitter layers producing photoexcited carriers. The carriers then undergo internal photoemission across the interface between the layers, and are swept out of the active region by the applied field, and collected at the contact. There are two contributions to the workfunction: i) the bandgap narrowing due to the doping in the emitters which occurs for both HIWIPs and HEIWIPs, and ii) the bandgap offset due to composition difference which occurs only in the HEIWIPs. The zero response threshold frequency is given by $f_0 = 0.242\Delta$ with f_0 in THz and the workfunction Δ in meV.

If GaAs emitters and AlGaAs barriers were used as is typically done in QWIPs or HEIWIPs designed with a higher frequency threshold, the two contributions to the workfunction would add together as shown in Fig. 1(a). The Al fraction x can be reduced to any value in theory. However, a practical lower limit will be around $x \geq 0.005$ with $f_0 \geq 2.7$ THz. (Although x = 0 is practical, then the device will no longer be a HEIWIP, and will have a $\sim$ 9 meV offset for $N_A = 3 \times 10^{18}$

cm^{-3} giving $f_0 = 2.17$ THz.) Although Δ_d can be reduced by increasing the doping, difficulties in controlling the doping and potential limits due to light-heavy hole transitions[8] make this approach unappealing. Further decrease in f_0 below 2.7 THz (i.e. beyond ~ 110 μm) requires a change in the design due to the minimum $\Delta = \Delta_d$ imposed by the bandgap narrowing.

One possible approach to avoid this limit is to use AlGaAs as the emitter and GaAs as the barrier. A partial band diagram of a THz HEIWIP detector is shown in Fig. 1(b). A key feature of this structure is the use of AlGaAs in the emitters and GaAs in the barriers. This is done in order to reduce the workfunction and obtain THz response. In such a device, the bandgap narrowing in the doped AlGaAs will be partially offset by the increased bandgap of the AlGaAs material relative to the GaAs as seen in Fig. 1, giving $\Delta = \Delta_d - \Delta_x$. For example, a $f_0 = 0.9$ THz (335 μm) detector would have an Al fraction of ~ 0.012. Based on calculations and measurements on doped AlGaAs films,[9] the FIR absorption in AlGaAs is expected to be very similar to GaAs, due to the very low Al content giving performances similar to the current devices with AlGaAs barriers.

One possible method of increasing the response is through the use of resonant cavity effects[10], [11]. The idea of the cavity architecture is to use the reflection from the top and bottom surfaces to create a standing wave in the device. Placing the emitters at the antinodes in the resulting resonant cavity structure will increase absorption and enhance the response at the resonant wavelengths. Resonant cavity effects have already been demonstrated in the reflection, transmission and absorption of structures even with semi-insulating substrates[12] and in detectors grown on doped substrates.[13] A complete model detailing the calculation of response including the cavity effect is given elsewhere.[14]

II. Experiment

A. Detector Design and Fabrication

The detector structure consisted of 10 periods of 3×10^{18} cm^{-3} Be-doped 500 Å thick $Al_{0.005}Ga_{0.995}As$ emitter and 2000 Å thick GaAs barrier sandwiched between two contacts. The top and bottom contacts are 1×10^{19} cm^{-3} Be-doped 500 Å and 7000 Å thick $Al_{0.005}Ga_{0.995}As$ layers, respectively. The detectors were fabricated by using wet etching techniques to isolate 400×400 to 1000×1000 μm^2 mesas and depositing Ti/Pt/Au ring contacts to allow for frontside illumination. As the devices use free-carrier absorption, normal incidence illumination can be used.

B. Dark Current

The devices were first characterized by measuring the dark current at 4.2 K, which showed good uniformity between devices with less than 5% variation in dark current density between mesas. Both the dark current and the photocurrent when exposed to a 300 K background were measured for various temperatures, and a BLIP temperature of 20 K was obtained. The dark current at different temperatures was also used to obtain the workfunction from an Arrhenious plot. The workfunction decreased with bias as shown in Fig. 2, which is believed to be due to band bending. The sharp jumps in Δ with bias were observed in multiple samples but their origin is unexplained at this time.

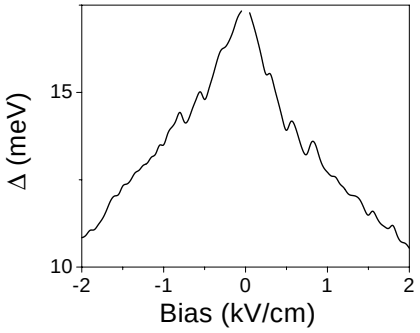

Fig. 2. The variation of the workfunction Δ with the applied bias. The effect is believed to be related to band bending from space charge in the barriers.

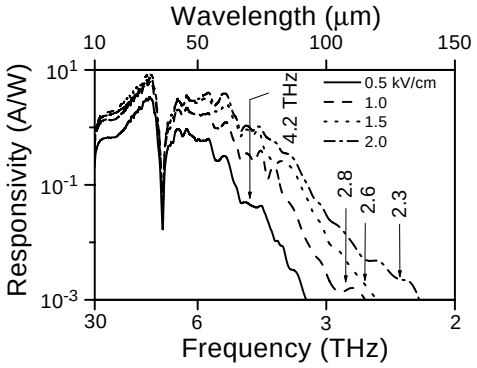

Fig. 3. The observed response for the THz detector. The peak response was at 9.6 THz with a responsivity of 7.3 A/W and $D^* = 5.3 \times 10^{11}$ Jones at 4.8 K and 2.0 kV/cm bias. The variation of f_0 with bias shown by the arrows is in good agreement with the values predicted from the arrhenious plots.

C. Spectra

The spectral response was measured at 4.2 K using a Fourier Transform Infrared (FTIR) spectrometer calibrated using a silicon composite bolometer. The results are shown in Fig. 3. Response was recorded from 30 THz to the threshold which varied with bias. The spectral threshold was in good agreement with the values predicted from the Arrhenious plot. This indicates that the electrical and optical barriers are the same. The predicted f_0 for this design was ~ 1.5 THz (200 μm) while the observed value was only 2.3 THz. This difference is believed to be related to the variation in Δ observed from the arrhenious plot caused by band bending. For detectors with thresholds below 3 THz the bending has become more important and future designs will consider methods of offsetting its effects, possibly by increasing the Al fraction.

The detectors were designed (for a total device thickness near 3 μm) with the first order cavity peak at ~ 7.5 THz which is near the decrease in absorption due to the reststrahlen band. Increasing the device thickness would increase the response

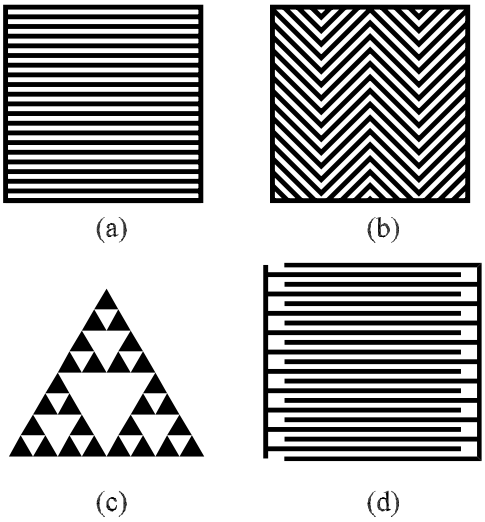

Fig. 4. Examples of the metal film patterns planned for testing. (a) A uniform grid to look for a polarized response. (b) A series of line segments to obtain a polarization independent response. (c) A Sierpinski gasket to test fractal patterns for a broad response. (d) An interdigitated contact to test the effects of a modulated lateral field on the plasmon resonances.

at longer wavelengths but would also be impractical for MBE growth. For example, a device optimized for $f_0 = 1$ THz with a cavity peak at 1.5 THz would require a total device thickness near 15 μm.

III. Plasmon Enhanced Detectors

Electromagnetic waves at metal-dielectric or metal-semiconductor interfaces, such as surface plasmon polaritons (SPPs), and SPs, have remarkable properties of generating highly enhanced local fields. These local fields in nanostructured systems can exceed excitation fields by orders of magnitude and undergo giant fluctuations in space and in time. These giant local fields are responsible for a multitude of enhanced optical phenomena and their applications. One of the most important and frequently used for applications, in physics, chemistry, molecular biology, medicine, and homeland security and national defense, is the Surface Enhanced Raman Scattering (SERS), gigantically enhanced Raman scattering from molecules adsorbed at metal nanosystems or in a vicinity of a metal system. The SERS is approximately proportional to $|E|^4$, where E is the local optical electric field in the units of the excitation field (i.e., E is the local field-enhancement factor). Typically, $E \sim Q = -\Re(\epsilon)/\Im(\epsilon) \sim 10$ - 100 for noble metals in the visible to IR region. Correspondingly, SERS is expected to be enhanced by factor of $G_{SERS} \sim 10^4$ - 10^8. This is the case for most of the experimental observations. However, under certain conditions, namely for molecules adsorbed on fractal clusters of colloidal silver, the enhancement is so large that SERS by single molecules can be seen. In this case the SERS enhancement is much larger, $G_{SERS} \sim 10^{12}$ - 10^{14}.

Enhancing detector performance by placing metal or semiconductor nanostructures in the vicinity of the electron-gas region of the detectors could lead to enhanced detector performance. The metal nanostructures will act as enhanced couplers, which will allow more efficient absorption of light as it is converted into surface plasmons (SPs). In the near field region, the electric field of the SPs will be enhanced over the incident radiation field. The near field of SPs will affect the electron gas in the photodetectors the same way as the far-field does. Thus the local field enhancement known for other phenomena and devices could be achieved. Surface plasmon enhanced absorption has been shown in the visible with "gold-blacks" and "silver-blacks" having absorption over 95%.[15] The idea is to employ this enhancement in the THz range. The near-field enhancement can be further increased by the use of self-similar patterns or tapered waveguides to concentrate the electric field in localized spatial regions. A simple self-similar nanosphere nanolens (known as a "snowman" nanolens) consists of a self-similar sequence of nanospheres with progressively decreasing radii and separations. For a symmetric six-nanosphere nanolens, the electric field enhancement is $\sim 10^3$.[16] A tapered waveguide also showed enhancement.[17] An alternate approach considered is the use of a periodic grating structure to produce plasmonic enhancements. Decreasing the grating spacing would increase the resonance frequency. This approach has already been applied with a grating on a double quantum well transistor detector for GHz radiation.[18] Such a grid could be used as a polarization-sensitive detector. By using a chevron-shaped grid or a fractal pattern, a non-polarization sensitive detector could be obtained. Some potential grid patterns are shown in Fig. 4.

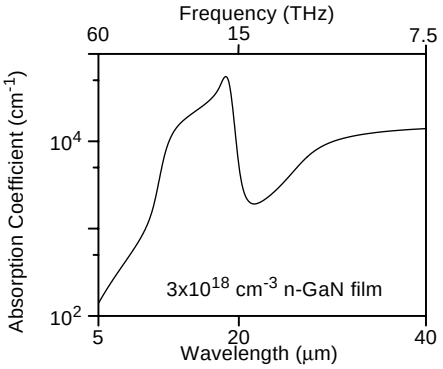

Fig. 5. Absorption coefficient for n-doped GaN film calculated from the reflection measurements.

IV. Other Materials

The use of materials other than GaAs can offer specific advantages to compensate for their disadvantage in material development. The well developed technology and ability to vary the Al fraction over a wide range due to the lattice matched nature of GaAs and AlAs have made the GaAs/AlGaAs material system a good choice during the development of these detectors. Other systems however, can provide advantages in certain ranges. Going to wider bandgap systems such as the

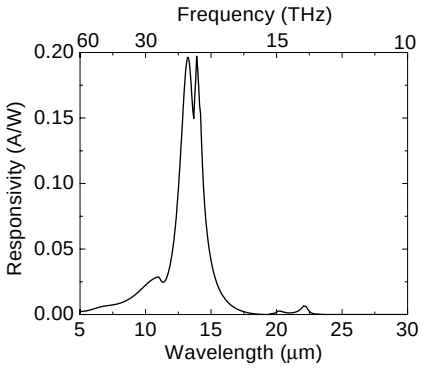

Fig. 6. The calculated response for a GaN/$Al_{0.02}Ga_{0.98}N$ detector with 10 layers calculated for a field of 1 kV/cm with the gain taken as 1. The device should have a BLIP temperature near 40 K.

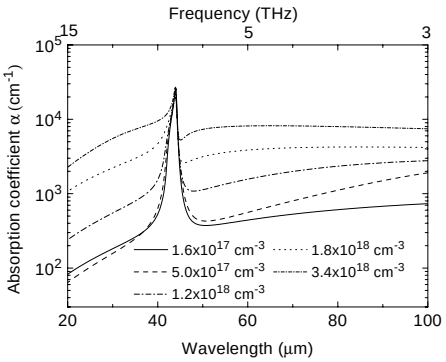

Fig. 7. Absorption coefficient for a GaSb film obtained from the reflection measurements.

nitrides and phosphides would improve radiation hardness. The increased bandgap would also mean that dual band detectors which would operate at higher frequencies could be designed. In particular, AlGaN would allow operation in the UV without responding to the visible.

1) GaN/AlGaN: The absorption of doped GaN films were obtained by measuring the reflection of GaN films grown on a sapphire substrate. The material parameters of the film were obtained by fitting the reflection to a model, and the resulting parameters were used to calculate the absorption coefficient shown in Fig. 5. This approach was used as the sapphire substrate does not transmit radiation above 6 μm, making a direct measurement of the absorption impossible. This could be used to design detectors for frequencies above 7.5 THz. While the response from the highest absorption value near 17 THz will be reduced due to reflection associated with the reststrahlen band, there will still be strong response in the range of 20-24 THz. The response of a GaN/AlGaN detector with Al fraction $x = 0.02$ is shown in Fig. 6 with a peak value of 0.2 A/W for a bias field of 1 kV/cm. This detector should operate up to $\sim$ 70 K with a BLIP temperature near 40 K. Due to the change in material the reststrahlen band has been moved to just near 17 THz making this a good alternative to GaAs/AlGaAs near 7.5 THz. A GaN based detector also would be likely to be more radiation hard due to the larger bandgap.

2) GaSb/InGaSb: The use of GaSb/GaInSb is of interest specifically for frequencies below 3 THz as better control of the workfunction is possible due to the much lower value of Δ_x in this system. In a GaAs/AlGaAs detector, $\Delta_x = 530$ meV while for GaSb/InGaSb $\Delta_x \sim 40$ meV. This much lower value means that unlike the GaAs/AlGaAs system in which the Al fraction is $< 1.7\%$ and must be controlled to 0.1% to obtain the desired thresholds, a GaSb/InGaSb detector would have In fractions near 15% allowing easier control. The disadvantage of this system is that the lattice mismatch will introduce defects which can reduce the detector efficiency. The absorption coefficient of doped GaSb films has been obtained using reflection measurements and are shown in Fig. 7.

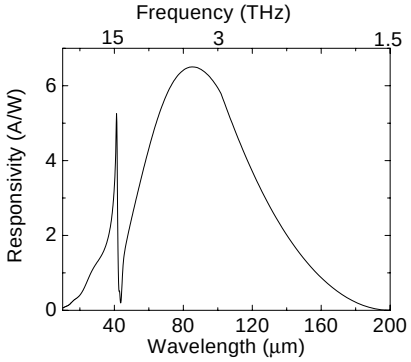

Fig. 8. The calculated response for a GaSb/$In_{0.2}Ga_{0.8}Sb$ detector with 30 layers calculated for a field of 1 kV/cm with the gain taken as 1.

Based on these results a detector with 30 periods using $In_{0.2}Ga_{0.8}Sb$ emitters and GaSb barriers has been modeled and the response is shown in Fig. 8. The peak response was 6 A/W at 3.1 THz for a bias field of 1 kV/cm. This detector is designed to operate at 4.2 K. The major advantage in this design is the large In fraction possible. For a similar threshold AlGaAs/GaAs design, an Al fraction of 0.010 would be needed with a corresponding high level of control.

V. Dual Band Response

One interesting possibility for these detectors is a dual band design in which both interband and intraband transitions are used.[19] By using two different transitions response is possible in very different spectral ranges. The basic design of a dual band detector using a single emitter and a barrier is shown in Fig. 9. The long wavelength operation is the same as for the standard IWIP detector, while the short wavelength response is via an interband transition. This mode of operation allows a device to operate in the THz range, and by choosing a material with the correct band gap, in the UV-NIR range. Preliminary measurements have been done using a GaAs HIWIP detector for which the interband transition is in the NIR range. The structure consists of a bottom contact (p^{++}) layer with 1.0 μm thickness, a barrier layer with 1.0 μm thickness, an emitter (p^{+}) layer with 0.2 μm thickness, and a top contact layer. During processing, the top contact and a part of the emitter

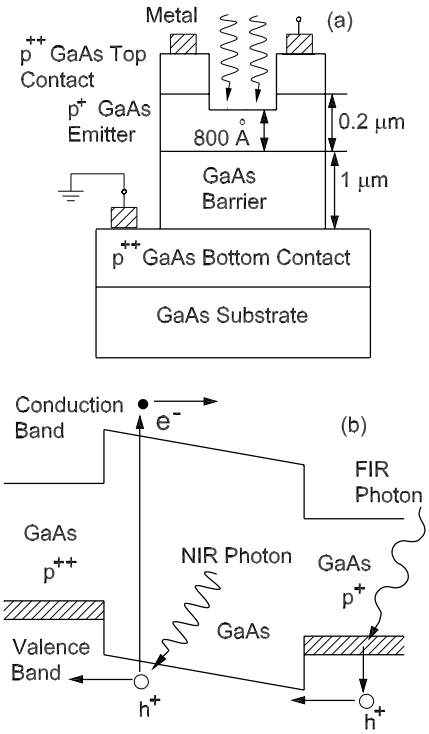

Fig. 9. (a) The detector structure as processed for use in the dualband measurements. Part of the top contact and emitter have been etched out to improve IR transmission into the detector. (b) The band diagram of the detector showing the two detection mechanisms. The THz detection occurs by an intraband transition in the bottom emitter, while the NIR detection occurs by an interband process in the barrier.

layer were etched out in the region inside the ring contact, leaving about 800 Å thick emitter region (out of 0.2 μm). The response obtained from the HIWIP detector is shown in Fig. 10. The response due to intraband transition is observed to 4.3 THz (70 μm) and it has a responsivity of $\sim$ 1.8 A/W and a detectivity of $\sim 5.6\times10^{10}$ Jones at 5.1 THz (57 μm) under 100 mV reverse bias. The peaks at 57 and 63 μm are due to transitions in the hydrogenic states of the impurity atoms present in the barrier. The interband response was observed at wavelengths below 0.8 μm. An optimum responsivity of $\sim$ 8 A/W and a detectivity of $\sim 6\times10^{9}$ Jones were obtained at 0.8 μm. By changing the material, the short wavelength response could be tailored to the desired range. One possibility for a dual band detector would be to use GaN/AlGaN with an interband transition in the UV giving a device which responds in both the UV and THz while ignoring the visible.

VI. Conclusion

The extension of HEIWIP response to $f_0 = 2.3$ THz has been demonstrated with a response of 7.3 A/W and $D^* = 5.3 \times 10^{11}$ Jones by the use of AlGaAs emitters and GaAs barriers. The response could be increased by the use of metal nanostructures to create plasmon effects. A dual band detector responding in the NIR and THz range was demonstrated based on using both interband and intraband transitions. As future developments, the use of alternate materials, GaN/AlGaN in a

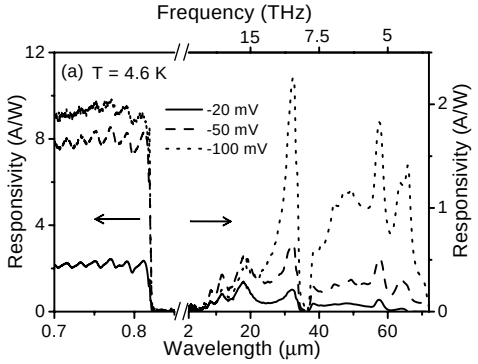

Fig. 10. Measured responsitivy for the dual band GaAs detector.

dual band structure to allow UV detection and GaSb/InGaSb for better control of the workfunction in THz designs were suggested. The absorption of both these materials was obtained and is similar to that of GaAs indicating their suitability.

Acknowledgment

This work was supported in part by the NSF under grants #ECS-0140434 and DBI: 0352324.

References

[1] H. A. Chu, M. T. Gardner, W. Hillier, and G. T. Babcock, Photosyn. Res. **66**, 57 (2000).
[2] H. A. Chu, H. Sackett, and G. T. Babcock, Biochem. **39**, 14371 (2000).
[3] J. Breton, E. Nabedryk, and A. Clerici, Vibrational Spectroscopy **19**, 71 (1999).
[4] H.C. Liu, C.Y. Song, A.J. Spring Thorpe, and J.C. Cao, Appl. Phys. Lett. **84**, 4068 (2004).
[5] A. G. U. Perera, H. X. Yuan and M. H. Francombe, J. Appl. Phys. **77**, 915 (1995).
[6] D. G. Esaev, M. B. M. Rinzan, S. G. Matsik, A. G. U. Perera, H. C. Liu, B. N. Zhonkov, V. I . Gavrilenko, and A. A. Belyanin, J. Appl. Phys. **95**, 512 (2003).
[7] A. G. U. Perera, S. G. Matsik, B. Yaldiz, H. C. Liu, A. Shen, M. Gao, Z. R. Wasilewski and M. Buchanan, Appl. Phys. Lett **78**, 2241 (2001).
[8] A. G. U. Perera, S. G. Matsik, M. B. M. Rinzan, A. Weerasekara, M. Alevli, H. C. Liu, M. Buchanan, B. Zvonkov, and V. Gavrilenko, Infrared Phys. Technol. **44**, 347 (2003).
[9] M. B. M. Rinzan, D. G. Esaev, A. G. U. Perera, S. G. Matsik, G. Von Winckel, A. Stintz, and S. Krishna, Appl. Phys. Lett. **85**, 5236 (2004).
[10] A. L. Korotkov, A. G. U. Perera, W. Z. Shen, H. C. Liu, M. Buchanan, Solid State Electronics **45**, 87 (2001).
[11] D. G. Esaev, S. G. Matsik, M. B. M. Rinzan, A. G. U. Perera, H. C. Liu, and M. Buchanan, J. Appl. Phys. **93**, 1879 (2003).
[12] A. L. Korotkov, A. G. U. Perera, W. Z. Shen, J. Herfort, K. H. Ploog, W. J. Schaff, and H. C. Liu, J. Appl. Phys **89**, 3295 (2001).
[13] S. G. Matsik, M. B. M. Rinzan, D. G. Esaev, A. G. U. Perera, G. von Winckel, A. Stintz, S. Krishna, H. C. Liu, M. D. Byloos, T. Oogarah, G. I. Sproule, K. Liu, and M. Buchanan, IEEE Transanctions Electron Devices **52**, 413 (2005).
[14] D. G. Esaev, M. B. M. Rinzan, S. G. Matsik, and A. G. U. Perera, J. Appl. Phys. **96**, 4588 (2004).
[15] C.-M. Wang, Y.-C. Chen, M.-S. Lee, and K.-J. Chen, Jpn. J. Appl. Phys. **39**, 551 (2000).
[16] K. Li, M. I. Stockman, and D. J. Bergman, Phys. Rev. Lett. **91**, 227402-1-4 (2003).
[17] M. I. Stockman, Phys. Rev. Lett. **93**, 137404 (2004).
[18] V. V. Popov, T. V. Teperik, O. V. Polischuk, X. G. Peralta, S. J. Allen, N. J. M. Horing, and M. C. Wanke, Phys. Solid State **46**, 153 (2004).
[19] G. Ariyawansa M. B. M. Rinzan D. G. Esaev S. G. Matsik A. G. U. Perera H. C. Liu B. N. Zvonkov V. I. Gavrilenko, Appl. Phys. Lett. **86**, 143510-3 (2005).